Belle DRAFT: *YY-NN*
Intended Journal: *PRD*
Authors: YoungJun Kim, Jung Keun Ahn, and Seongbae Yang
Committee: John Yelton (chair), Masayuki Niiyama, and Elena Solovieva
Belle Note No.: 1554
Version: 2.12, Date: June 12, 2024

Measurement of the Branching Fraction of $\Lambda_c^+ \to pK_S^0\pi^0$ at Belle

We report a precise measurement of the ratio of branching fractions $\mathcal{B}(\Lambda_c^+ \to pK_S^0\pi^0)/\mathcal{B}(\Lambda_c^+ \to pK^-\pi^+)$ using 980 fb^{-1} of e^+e^- collision data from the Belle experiment. We obtain a value of $\mathcal{B}(\Lambda_c^+ \to pK_S^0\pi^0)/\mathcal{B}(\Lambda_c^+ \to pK^-\pi^+) = 0.339 \pm 0.002 \pm 0.009$, where the first and second uncertainties are statistical and systematic, respectively. This measurement is consistent with the previous measurement from the CLEO experiment but has a fivefold improvement in precision. By combining our result with the world average $\mathcal{B}(\Lambda_c^+ \to pK^-\pi^+)$, we obtain the absolute branching fraction $\mathcal{B}(\Lambda_c^+ \to pK_S^0\pi^0) = (2.13 \pm 0.01 \pm 0.05 \pm 0.11)\%$, where the uncertainties are statistical, general systematic, and specific systematic due to the uncertainty in $\mathcal{B}(\Lambda_c^+ \to pK^-\pi^+)$, respectively. This measurement can shed light on hadronic decay mechanisms in charmed baryon decays.

I. INTRODUCTION

The nonleptonic weak decays of Λ_c^+ provide a unique testing ground for understanding the factorization scheme involving the $c \to s$ transition and the final-state interactions. Among the possible final states, $N\bar{K}\pi$ decays are particularly useful for examining the isospin properties of the weak interaction in Λ_c^+ decay [1]. The $\Delta S = 1$ Cabibbo-allowed transition is governed by $c \to su\bar{d}$, so iso-singlet Λ_c^+ decays result in a final state with $I = I_3 = 1$. In the $\Lambda_c^+ \to N\bar{K}\pi$ decays, the $N\bar{K}$ state can have isospin 0 or 1. Thus, the sum of isospin amplitudes of the three decay modes, $\sqrt{2}\mathcal{A}(p\bar{K}^0\pi^0) + \mathcal{A}(pK^-\pi^+) + \mathcal{A}(n\bar{K}^0\pi^+)$, is zero according to isospin symmetry [2–4], which imposes useful constraints on the branching ratios of the nonleptonic decay channels. In the quark-diagram schemes for $\Lambda_c^+ \to N\bar{K}\pi$ decays, as shown in Fig. 1, direct π^+ emission can involve a color-allowed factorizable process with external W^+ emission (Fig. 1(c)) but a π^0 cannot be produced in this process. The dominant contributions in the $N\bar{K}\pi^0$ decays instead come from color-suppressed internal W^+ emission and internal flavor conversion involving the subprocess $cd \to su$ with W^+ exchange.

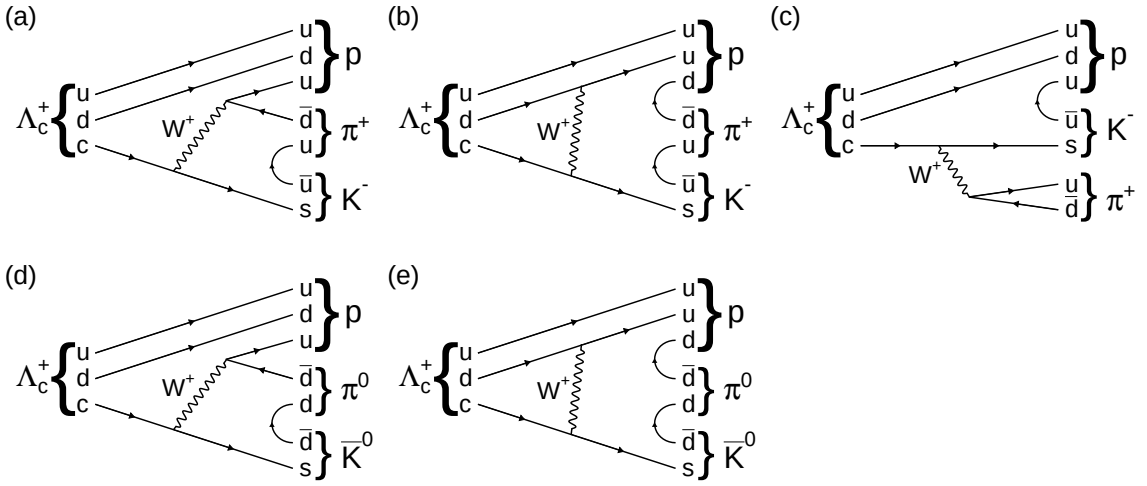

FIG. 1. Typical Feynman diagrams for internal W emission processes in $\Lambda_c^+ \to pK^-\pi^+$ (a) and $\Lambda_c^+ \to pK_S^0\pi^0$ (d), internal W exchange processes in $\Lambda_c^+ \to pK^-\pi^+$ (b) and $\Lambda_c^+ \to pK_S^0\pi^0$ (e), and external W emission process in $\Lambda_c^+ \to pK^-\pi^+$ (c).

Since direct π^+ emission leaves the ud diquark in the iso-singlet Λ_c^+ as a spectator, the sud cluster in the final state is a pure $I = 0$ state, thus favoring the $I = 0$ $\bar{K}N$ state [5, 6]. Hence, if the direct π^+ emission process is dominant, the two-body decay $\Lambda_c^+ \to \Lambda\pi^+$ should be greatly favored over $\Lambda_c^+ \to \Sigma^0\pi^+$. Moreover, as the Λ_c^+ contains an anti-symmetric quark pair $(ud - du)c$, factorizable processes are suppressed for Λ_c^+ decays involving a baryon decuplet with totally flavor symmetric quark content [7]. However, the experimentally determined branching fractions for the two decays are comparable, indicating that the contributions from color-suppressed W^+ emission and W^+ exchange processes are large. The subsequent rescattering of the $N\pi$ pair can populate $N(1535)$ and $N(1650)$ resonances, and the $N\bar{K}$ final-state interaction generates $\Lambda(1405)$ and $\Lambda(1670)$ states [8].

An observation of a narrow structure at the $\Lambda\eta$ threshold in the K^-p invariant mass spectrum in $\Lambda_c^+ \to pK^-\pi^+$ reported by the Belle collaboration [9] has attracted significant attention. A recent analysis, attempting to shed light on the nature of the structure, indicates a $\Lambda\eta$ cusp effect, enhanced by the $\Lambda(1670)$ pole [10]. Another study suggests that the effect giving rise to the narrow structure is enhanced by a triangle singularity involving rescattering via the near-lying $\Lambda a_0(980)^+$ or $\eta\Sigma(1660)^+$ scattering [11]. In $\Lambda_c^+ \to pK^-\pi^+$ process, isospin symmetry implies that the partial branching ratio of $\Lambda_c^+ \to \Sigma^{*+}\pi^0$ equals that of $\Lambda_c^+ \to \Sigma^{*0}\pi^+$, whereas the $\Lambda_c^+ \to \Delta^{++}K^-$ decay is three times larger than the

branching fraction of $\Lambda_c^+ \to \Delta^+ \bar{K}^0$ [7, 12]. In the $\Lambda_c^+ \to p\bar{K}^0\pi^0$ decay, only Σ^{*+} resonances are possible in the $N\bar{K}$ system. Therefore, a precise measurement of the relative branching fraction for $\Lambda_c^+ \to pK_S^0\pi^0$ as well as the investigation of intermediate resonances provides stringent tests of isospin symmetry and could help to better understand non-factorizable processes in the non-leptonic decay of charmed baryons.

The absolute branching fractions for $\Lambda_c^+ \to n\bar{K}^0\pi^+$ and $\Lambda_c^+ \to pK_S^0\pi^0$ decays are reported from BESIII to be $\mathcal{B}(\Lambda_c^+ \to nK_S^0\pi^+) = (1.82\pm0.25)\%$ and $\mathcal{B}(\Lambda_c^+ \to pK_S^0\pi^0) = (1.87\pm0.14)\%$, respectively [3]. The branching fraction of $\Lambda_c^+ \to pK_S^0\pi^0$ relative to $\Lambda_c^+ \to pK^-\pi^+$ reported from CLEO is 0.33 ± 0.05 [13]. This paper reports a precise measurement of the relative branching fraction of $\Lambda_c^+ \to pK_S^0\pi^0$ compared with $\Lambda_c^+ \to pK^-\pi^+$ using Belle data. In addition, we present the first investigation of the intermediate resonances in $\Lambda_c^+ \to pK_S^0\pi^0$ decays.

II. THE DATA SAMPLE AND THE BELLE DETECTOR

The branching fractions are measured based on a full data sample obtained at or near $\Upsilon(1S)$, $\Upsilon(2S)$, $\Upsilon(3S)$, $\Upsilon(4S)$ and $\Upsilon(5S)$ with the Belle detector at the KEKB asymmetric energy e^+e^- collider [14]. The full data sample has an integrated luminosity of 980 fb^{-1}. The Belle detector was a large-solid-angle magnetic spectrometer comprising a silicon vertex detector (SVD), a central drift chamber (CDC), an array of aerogel threshold Cherenkov counters (ACC), a barrel-like arrangement of time-of-flight scintillation counters (TOF), and an electromagnetic calorimeter comprising CsI(Tl) crystals (ECL) located inside a superconducting solenoid that provided a 1.5 T magnetic field. An iron flux return located outside the coil was employed to detect K_L^0 mesons and identify muons. The Belle detector is described in detail in Ref. [15].

The Monte Carlo (MC) samples used in the simulation studies are generated using EvtGen [16] and PYTHIA [17], and propagated through a virtual GEANT3 model of the full detector [18]. The final-state radiation process is simulated using the PHOTOS [19] package in EvtGen. A signal MC sample is generated via $e^+e^- \to c\bar{c} \to \Lambda_c^+ + X$ to study the reconstruction efficiency and signal shape functions. A Belle generic MC sample including $\Upsilon(4S) \to B\bar{B}$, $\Upsilon(5S) \to B_{(s)}^{(*)}\bar{B}_{(s)}^{(*)}$, $\Upsilon(1S, 2S, 3S)$ decays and $e^+e^- \to q\bar{q}$ ($q = u, d, s, c$) with the same integrated luminosity as the real data is used to optimize the selection criteria.

III. EVENT SELECTION

We consider the $\Lambda_c^+ \to pK_S^0\pi^0$ process with subsequent decays $K_S^0 \to \pi^+\pi^-$ and $\pi^0 \to \gamma\gamma$. The event selection criteria are optimized using a generic MC sample, with a figure-of-merit (FoM) defined as $N_{\rm sig}/\sqrt{N_{\rm sig}+N_{\rm bkg}}$, where $N_{\rm sig}$ is the number of signal events and $N_{\rm bkg}$ is the number of background events. The latter are obtained in the $pK_S^0\pi^0$ invariant mass region between 2.263 GeV/c^2 and 2.306 GeV/c^2.

The likelihood $\mathcal{L}_i$ ($i = \pi^\pm,\ K^\pm,\ p^\pm$) is calculated by combining information from the ACC, CDC, and TOF detectors. The likelihood ratio between hypotheses i and i' is defined as $\mathcal{R}(i|i') = \mathcal{L}_i/(\mathcal{L}_i + \mathcal{L}_{i'})$. Charged tracks must satisfy $\mathcal{R}(p|K) > 0.9$ and $\mathcal{R}(p|\pi) > 0.9$ to be considered as proton candidates. Furthermore, the electron likelihood ratio ($\mathcal{R}(e)$), obtained from ACC, CDC, and ECL information, should be smaller than 0.9 for the proton candidates. In addition, the distance-of-closest-approach (DOCA) to the beam interaction point (IP) must be smaller than 2.0 cm along the beam direction (z) and smaller than 0.1 cm in the transverse direction (r). Furthermore, at least one hit in SVD is required. After applying the selection criteria, the PID efficiency for the proton candidates is 83% in the typical momentum range of the decays.

We reconstruct K_S^0 candidates from $K_S^0 \to \pi^+\pi^-$ decays, which are identified using a neural network algorithm involving the K_S^0 momentum in the laboratory frame, the distance between two charged pion tracks along the z axis, the flight length of K_S^0 projected onto the r plane, the angle between the K_S^0 momentum and the vector from IP to K_S^0 decay vertex in the laboratory frame, longer and shorter DOCAs in the r-direction of charged pions, the angle between the K_S^0 momentum in the laboratory frame and charged the pion momentum in the K_S^0 rest frame, the number of CDC hits from each $\pi^\pm$ track and the presence or absence of SVD hits [20]. In addition, we perform a mass-constrained fit to the K_S^0 candidates in order to improve the momentum resolution. The χ^2 value of the mass-constrained vertex fit to the π^+ and π^- tracks with a common vertex is required to be smaller than 40.

ECL clusters that do not have matching tracks in the CDC are identified as photons, and the π^0 candidates are reconstructed from photon pairs. For each photon, the energy deposited in the ECL must exceed 50 (100) MeV if the cluster is found in the barrel (end-cap) region [15]. The ratio of energy deposits in the 3×3 array of crystals, centered in the crystal with the highest energy, to that of 5×5 crystal array must exceed 0.9. We

select the π^0 candidates within the $M(\gamma\gamma)$ range from 120 MeV/c^2 to 150 MeV/c^2. The momentum of the π^0 candidate must be greater than 400 MeV/c in the laboratory frame. A mass-constrained fit is also performed on the π^0 candidates to improve their momentum resolution, requiring the χ^2 value of the fit to be smaller than 100.

As a final step, the proton, K^0_S, and π^0 candidates are combined to reconstruct Λ_c^+ candidates. The scaled momentum x_p is defined as $x_p = p^* c/\sqrt{s/4 - M^2c^4}$, where p^* is the momentum of the Λ_c^+ candidate in the center-of-mass frame, s is the square of the beam center-of-mass energy and M is invariant mass of the Λ_c^+ candidate. The requirement of $x_p > 0.54$ reduces the combinatorial background, particularly from the B meson decay. We perform a vertex fit to the three decay products requiring a common vertex. The χ^2 value of the vertex fit is required to be smaller than 40.

For $\Lambda_c^+ \to pK^-\pi^+$ decays, we reconstruct Λ_c^+ candidates using the event selection criteria typically used in other Λ_c^+ analyses with Belle [9], except that the x_p cut-off value is the same as in $\Lambda_c^+ \to pK^0_S\pi^0$ decays. For proton candidates, the same selection criteria are used as in our signal mode. For K^- and π^+ candidates, the requirements on $\mathcal{R}(e)$, DOCAs in z- and r-directions, and SVD hits are identical to those for proton candidates. However, the PID requirements are $\mathcal{R}(K|\pi) > 0.9$ and $\mathcal{R}(K|p) > 0.4$ for K^- and $\mathcal{R}(\pi|K) > 0.4$ and $\mathcal{R}(\pi|p) > 0.4$ for π^+. We fit the three decay products to a common vertex. The χ^2 value of the vertex fit is required to be smaller than 40.

After applying all the selection criteria to the data, we observe an average of 1.04 and 1.02 candidates per event for the $\Lambda_c^+ \to pK^0_S\pi^0$ and $\Lambda_c^+ \to pK^-\pi^+$ modes within the invariant mass ranges $2.263\,\mathrm{GeV}/c^2 < M(pK^0_S\pi^0) < 2.306\,\mathrm{GeV}/c^2$ and $2.274\,\mathrm{GeV}/c^2 < M(pK^-\pi^+) < 2.298\,\mathrm{GeV}/c^2$, respectively. In addition, we find that approximately 4.0% and 1.8% of events in these modes contain multiple signal candidates. Since these multiple candidates do not contribute to the peaking background in the generic MC simulation study, we retain all candidates for further analysis.

IV. SIGNAL EXTRACTION AND EFFICIENCY CORRECTION

Figure 2 shows the $M(pK^-\pi^+)$ and $M(pK^0_S\pi^0)$ distributions after applying the event selection method described in the previous section. We perform an extended maximum likelihood fit to extract the signal decay yields from the invariant mass distributions. The Λ_c^+

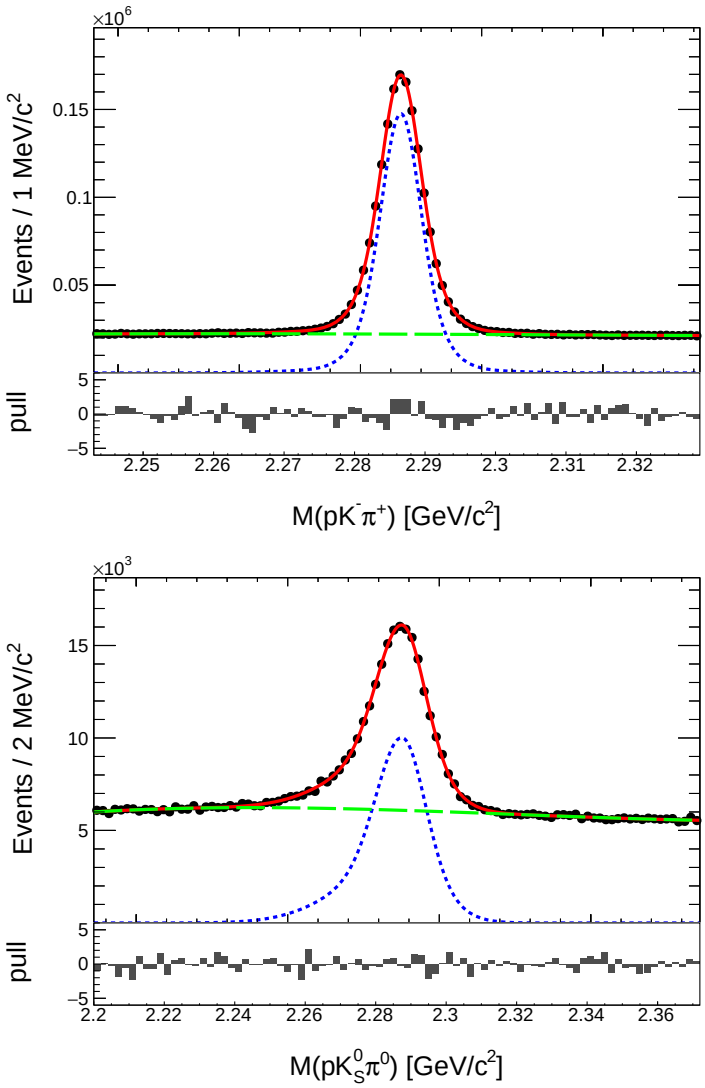

FIG. 2. Invariant mass distributions of Λ_c^+ candidates and fit results for $\Lambda_c^+ \to pK^-\pi^+$ (top) and $\Lambda_c^+ \to pK_S^0\pi^0$ (bottom). The total fit, signal, and background are shown by solid red, dashed blue, and long dashed green, respectively.

peak in the $M(pK^-\pi^+)$ distribution is parameterized by a sum of two Gaussian functions and one bifurcated Gaussian function, with each function sharing a common mean. To accurately model the energy loss associated with π^0 daughter γ's in the $\Lambda_c^+ \to pK_S^0\pi^0$ decay, its signal function is taken as the sum of two bifurcated Gaussian functions sharing a common mean. A third-order polynomial function represents the combinatorial backgrounds for $M(pK^-\pi^+)$ and $M(pK_S^0\pi^0)$ fits. The extracted Λ_c^+ yields for $\Lambda_c^+ \to pK^-\pi^+$ and $\Lambda_c^+ \to pK_S^0\pi^0$ decays are $(1.405 \pm 0.003) \times 10^6$ and $(1.283 \pm 0.010) \times 10^5$, respectively, where the uncertainties are

purely statistical.

The mass resolutions for $\Lambda_c^+ \to pK^-\pi^+$ decay are parameterized as follows: two Gaussians with σ values of (3.17±0.02) MeV/c^2 and (4.80±0.07) MeV/c^2 respectively, and a bifurcated Gaussian with $\sigma_{\rm left} = (19.5 \pm 0.39)$ MeV/c^2 and $\sigma_{\rm right} = (10.9 \pm 0.32)$ MeV/c^2. The yield fractions for the two Gaussians are (50.2±1.3)% and (42.3±0.6)%. For $\Lambda_c^+ \to pK_S^0\pi^0$ decay, there are two bifurcated Gaussians with $\sigma_{\rm left}$ and $\sigma_{\rm right}$ as follows: (8.19 ± 0.23) MeV/c^2 and (7.31 ± 0.27) MeV/c^2 for the first Gaussian, and (19.5 ± 0.22) MeV/c^2 and (11.6 ± 0.30) MeV/c^2 for the second Gaussian. The yield ratio between the two Gaussians is 1.07 ± 0.07. The uncertainties of these values are statistical only.

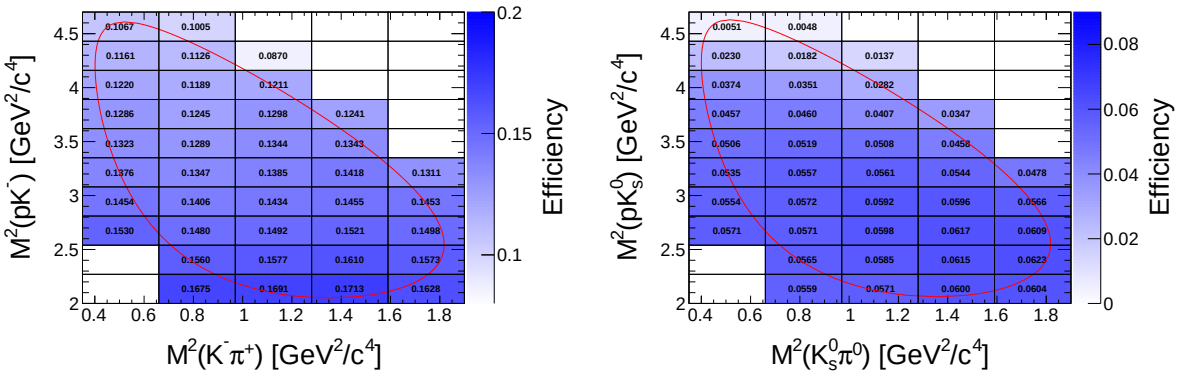

FIG. 3. Distributions of average reconstruction efficiencies over the Dalitz plots divided into the 10×5 bins of $M^2(pK)$ vs. $M^2(K\pi)$ for the $\Lambda_c^+ \to pK^-\pi^+$ (left) and the $\Lambda_c^+ \to pK_S^0\pi^0$ (right). Red contours represent the kinematic boundaries of the Dalitz plot, assuming the nominal Λ_c^+ mass.

As the reconstruction efficiency varies across the phase space of the Dalitz plot, as shown in Fig. 3, we perform a bin-by-bin correction to estimate the efficiency-corrected yields of both decays. To improve the resolution of the Dalitz plots, we fit the trajectories of the Λ_c^+ daughters to a common vertex and use a Λ_c^+ mass constraint. The efficiency-corrected yield y^{corr} calculated via $y^{corr} = \sum_i \frac{y_i}{\epsilon_i}$, where y_i and ϵ_i are the extracted yield and reconstruction efficiency of i-th bin in the Dalitz plots, respectively. In this correction, the Dalitz plots are divided into 5×10 bins for both decays, as shown in Fig. 4. Note that the bin width of the Dalitz plots is much larger than the resolution of the data, so the effect of bin migration on y_i is negligible.

The yield for each bin is determined using the same functions employed for the overall

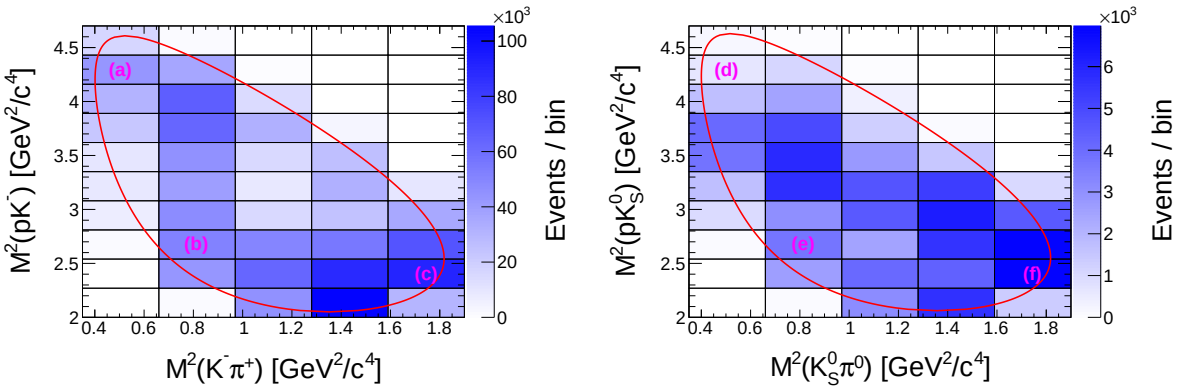

FIG. 4. Extracted signal yield for each Dalitz bin for $\Lambda_c^+ \to pK^-\pi^+$ (left) and $\Lambda_c^+ \to pK_S^0\pi^0$ (right). Fit results in the sample bins labeled from (a) to (f) are shown in Fig. 5. Red contours represent the Dalitz plot boundaries assuming the nominal Λ_c^+ mass.

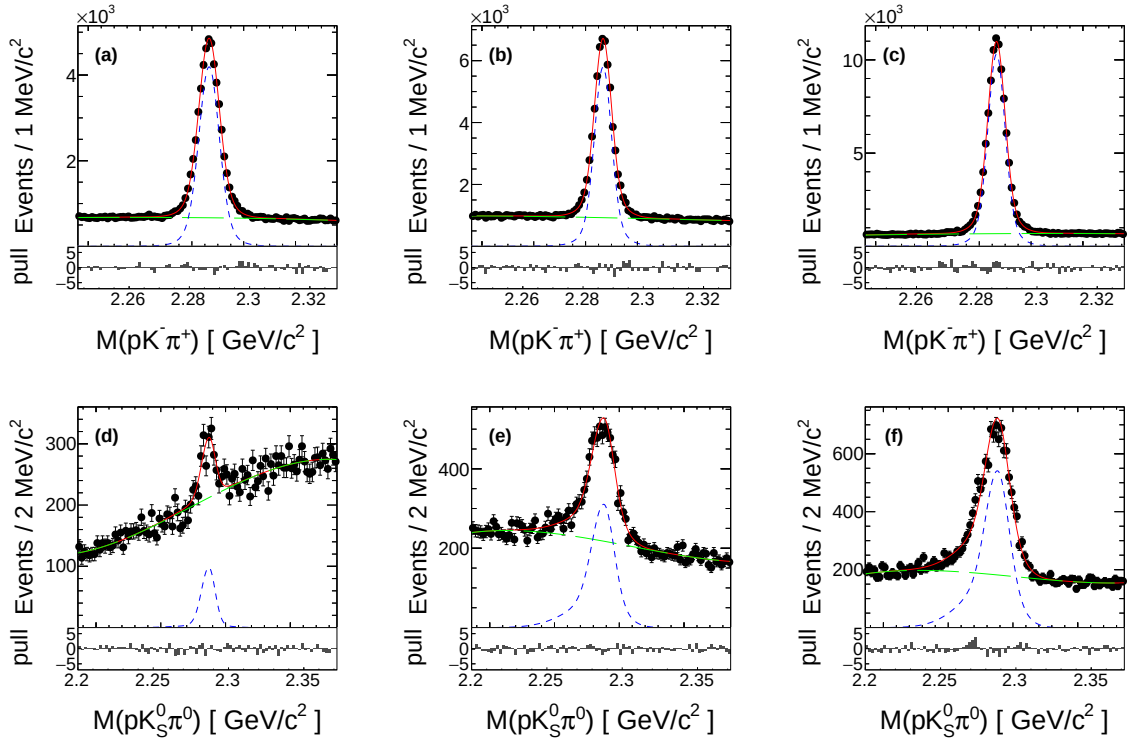

FIG. 5. Fit results (red curves) in the sample Dalitz plot bins specified in Fig. 4 for (a-c) $\Lambda_c^+ \to pK^-\pi^+$ and (d-f) $\Lambda_c^+ \to pK_S^0\pi^0$ decays. The dashed blue and long dashed green curves represent the signal and background, respectively.

event fit. However, all lineshape parameters, except for a common scaling factor applied to all Gaussian widths, are fixed at the values obtained from corresponding signal MC

samples. This scaling factor corrects for the resolution difference between the data and the MC simulation. The fitting results for typical bins are shown in Fig. 5. We determine the efficiency-corrected yields as $(9.570 \pm 0.012) \times 10^6$ for $\Lambda_c^+ \to pK^-\pi^+$ and $(2.221 \pm 0.015) \times 10^6$ for $\Lambda_c^+ \to pK_S^0\pi^0$, where the uncertainties are statistical only. The bin-by-bin correction method enables the extraction of efficiency-corrected yields, without requiring specific models for the production of intermediate states.

V. BRANCHING FRACTION

The relative branching fraction is calculated using the following equation,

$$\frac{\mathcal{B}(\Lambda_c^+ \to pK_S^0\pi^0)}{\mathcal{B}(\Lambda_c^+ \to pK^-\pi^+)} = \frac{y^{corr}(\Lambda_c^+ \to pK_S^0\pi^0)}{y^{corr}(\Lambda_c^+ \to pK^-\pi^+) \times \mathcal{B}(\pi^0 \to \gamma\gamma) \times \mathcal{B}(K_S^0 \to \pi^+\pi^-)}, \tag{1}$$

where we use $\mathcal{B}(\pi^0 \to \gamma\gamma) = (98.823 \pm 0.034)\%$ and $\mathcal{B}(K_S^0 \to \pi^+\pi^-) = (69.20 \pm 0.05)\%$ from Ref. [21]. By using the Eq. (1) and the efficiency-corrected yields, the relative branching fraction is determined as follows:

$$\frac{\mathcal{B}(\Lambda_c^+ \to pK_S^0\pi^0)}{\mathcal{B}(\Lambda_c^+ \to pK^-\pi^+)} = 0.339 \pm 0.002, \tag{2}$$

where the uncertainty is only statistical.

By assuming that the sum of the amplitudes, $\sqrt{2}\mathcal{A}(p\bar{K}^0\pi^0) + \mathcal{A}(pK^-\pi^+) + \mathcal{A}(n\bar{K}^0\pi^+)$, is zero as described above, we can express the amplitudes in terms of two components, $\mathcal{A}_0$ and $\mathcal{A}_1$, corresponding to the isospin amplitudes of the $I = 0$ and $I = 1$ states of the $N\bar{K}$ system, respectively [2, 3]. Defining a relative phase difference (δ), between $\mathcal{A}_0$ and $\mathcal{A}_1$ as $\mathcal{A}_1/\mathcal{A}_0 = |\mathcal{A}_1/\mathcal{A}_0|e^{i\delta}$, the branching fractions are expressed as following equations:

$$\mathcal{B}(\Lambda_c^+ \to p\bar{K}^0\pi^0) = \frac{1}{2}|\mathcal{A}_1|^2, \tag{3}$$

$$\mathcal{B}(\Lambda_c^+ \to pK^-\pi^+) = \frac{1}{2}|\mathcal{A}_0|^2 + \frac{1}{4}|\mathcal{A}_1|^2 - \frac{1}{\sqrt{2}}|\mathcal{A}_0||\mathcal{A}_1|\cos\delta, \tag{4}$$

and

$$\mathcal{B}(\Lambda_c^+ \to n\bar{K}^0\pi^+) = \frac{1}{2}|\mathcal{A}_0|^2 + \frac{1}{4}|\mathcal{A}_1|^2 + \frac{1}{\sqrt{2}}|\mathcal{A}_0||\mathcal{A}_1|\cos\delta. \tag{5}$$

With the measured value of $\mathcal{B}(\Lambda_c^+ \to pK_S^0\pi^0)/\mathcal{B}(\Lambda_c^+ \to pK^-\pi^+)$ and the world average $\mathcal{B}(\Lambda_c^+ \to n\bar{K}^0\pi^+)/\mathcal{B}(\Lambda_c^+ \to pK^-\pi^+) = 0.581 \pm 0.084$ [21], $|\delta|$ was determined to be

1.84 ± 0.07, while the relative strength ($|\mathcal{A}_1|/|\mathcal{A}_0|$) was found to be 1.23 ± 0.06, where the uncertainty is the sum in quadrature of the statistical uncertainty and the uncertainty in $\mathcal{B}(\Lambda_c^+ \to n\bar{K}^0\pi^+)/\mathcal{B}(\Lambda_c^+ \to pK^-\pi^+)$. The results show that the isospin amplitude $\mathcal{A}_1$ is not significantly suppressed compared to $\mathcal{A}_0$ in Λ_c^+ decays. Here, we note that the calculation considers only the isospin symmetry of non-resonant contributions [2].

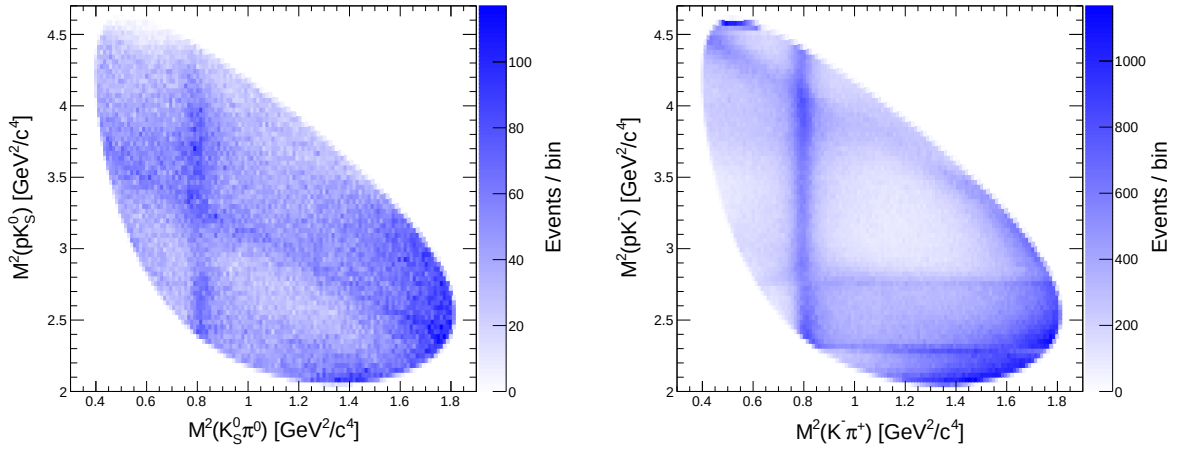

FIG. 6. Dalitz plots of the $\Lambda_c^+ \to pK_S^0\pi^0$ (left) and $\Lambda_c^+ \to pK^-\pi^+$ (right) channels within the regions 2.263 GeV/c^2 $< M(pK_S^0\pi^0) <$ 2.306 GeV/c^2 and 2.274 GeV/c^2 $< M(pK^-\pi^+) <$ 2.298 GeV/c^2, respectively. Both bin widths of x and y axes are 0.02 GeV$^2/c^4$. Non-Λ_c^+ background events shown in Fig. 2 are included in the Dalitz plots.

Figure 6 shows the Dalitz plot, $M^2(K_S^0\pi^0)$ vs. $M^2(pK_S^0)$ for $\Lambda_c^+ \to pK_S^0\pi^0$ decays, and several bands corresponding to intermediate resonances are observed in the plot. We investigate the intermediate resonances by projecting the Dalitz plot onto the one-dimensional distributions of $M(pK_S^0)$, $M(K_S^0\pi^0)$, and $M(p\pi^0)$. We apply efficiency corrections and then subtract non-Λ_c^+ background.

In the $M(pK_S^0)$ distribution and the Dalitz plot of the $\Lambda_c^+ \to pK_S^0\pi^0$, as shown in Fig. 7(a) and the left of Fig. 6, respectively, Σ^* hyperons are not as prominent. However, there are distinct peak structures that might be tentatively ascribed to $\Lambda(1520)$ and $\Lambda(1670)$ hyperons in the $M(pK^-)$ distribution, as shown in Fig. 7(b). This finding is in agreement with the expectation that Λ^* hyperons are preferred over Σ^* hyperons in the π^+ emission decays [5]. This could be attributed to their production dynamics being governed by color-suppressed factorizable process in the $\Lambda_c^+ \to pK_S^0\pi^0$ decay.

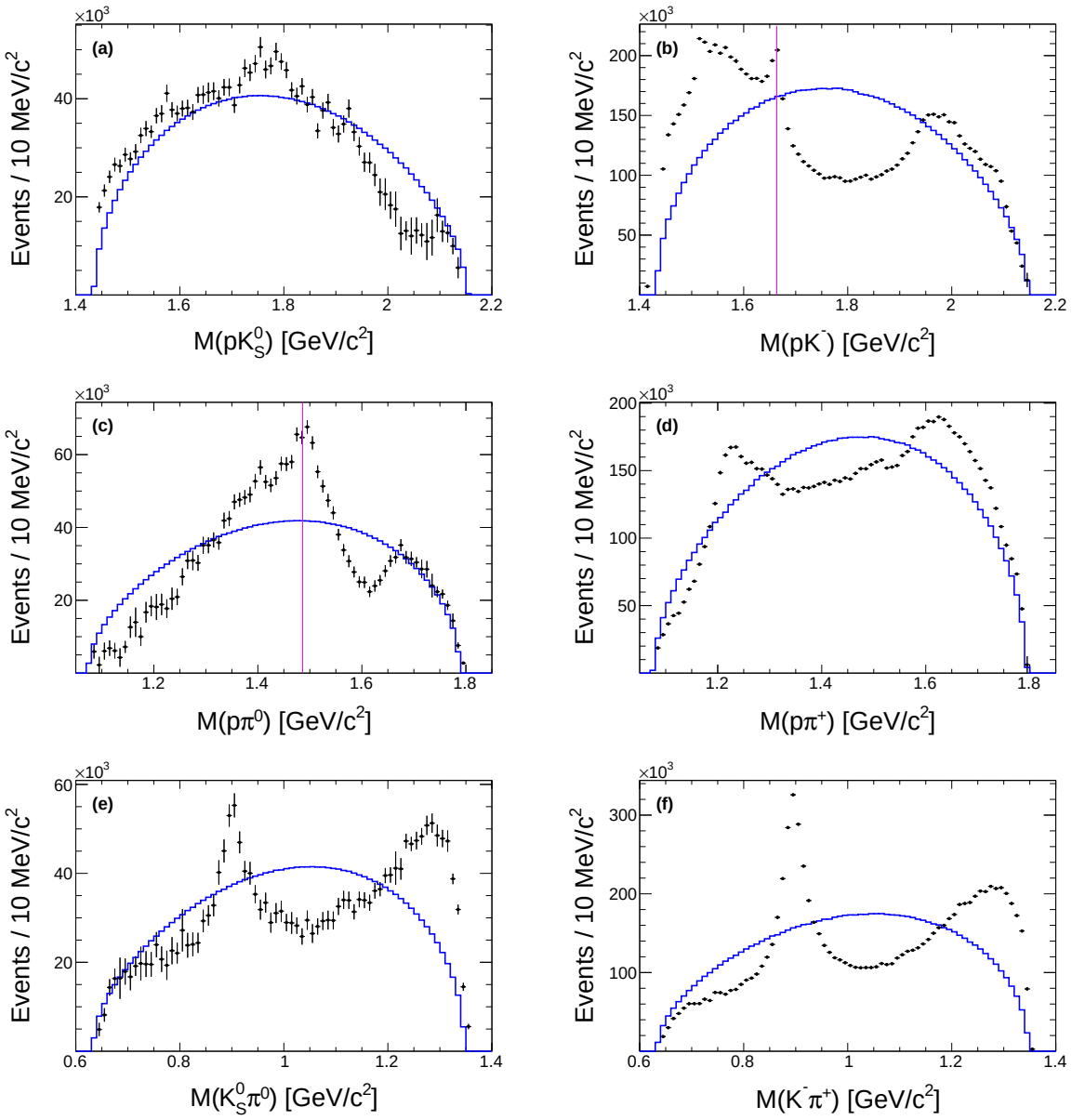

FIG. 7. Mass projection plots of $\Lambda_c^+ \to pK_S^0\pi^0$ (left) and $\Lambda_c^+ \to pK^-\pi^+$ (right) after background subtraction and efficiency correction. The projections of signal MC generated with a phase space model are superimposed in blue histograms. A clear peaking structure at the K^* resonance is seen in the $K_S^0\pi^0$ system (e), and a strong enhancement near the $p\eta$ mass threshold is found in (c). The $\Lambda\eta$ and $p\eta$ mass thresholds are marked in (b) and (c), respectively.

The peaking structure corresponding to $\Delta(1232)$ is much smaller in the $M(p\pi^0)$ distribution of the $\Lambda_c^+ \to pK_S^0\pi^0$ sample (Fig. 7(c)) compared to the one in the $M(p\pi^+)$ distribution for $\Lambda_c^+ \to pK^-\pi^+$ decays (Fig. 7(d)). This suppression can be attributed to the preference

for the production of the $\Delta^{++}K^-$ channel over the $\Delta^+\bar{K}^0$ channel, as required by isospin symmetry. Furthermore, a clear peaking structure near the $p\eta$ mass threshold is evident in the $M(p\pi^0)$ distribution of $\Lambda_c^+ \to pK_S^0\pi^0$ decay. This peak corresponds to the diagonal band observed in the Dalitz plot to the left of Fig. 6. The same effect was observed in the $\Lambda_c^+ \to pK_S^0\eta$ study in Ref. [22]. The similarity of this effect and the $\Lambda\eta$ threshold cusp, which was found to be amplified by the $\Lambda(1670)$ in the pK^- system as shown in Fig. 7(b) [10, 23], suggests that the peak near the $p\eta$ threshold in the Fig. 7(c) may also be attributed to a threshold cusp enhanced by the $N(1535)^+$.

Both $\Lambda_c^+ \to pK^-\pi^+$ and $\Lambda_c^+ \to pK_S^0\pi^0$ decays exhibit a peaking structure corresponding to the vector resonance $K^*(892)^0$, as shown in Fig. 7(e) and (f). In the region where high-mass K^* mesons are expected, a clear enhancement with respect to phase space is seen in both decay modes. To further understand the role of isospin symmetry in the Λ_c^+ decays and extend our understanding of intermediate states such as Λ^*, Σ^*, Δ^*, and N^* resonances, an amplitude analysis with the helicity formalism of these two channels is planned for the near future.

VI. SYSTEMATIC UNCERTAINTY

The systematic uncertainties of branching fractions are listed in Table I. The K_S^0 reconstruction imposes a systematic uncertainty that has been estimated using a control sample of $D^{*\pm} \to D^0\pi^\pm(D^0 \to K_S^0\pi^0)$ events. In the control sample study, the momentum-dependent K_S^0 reconstruction efficiency was compared between the data and MC samples. In a similar way, the π^0 reconstruction uncertainty was determined by a study in Ref. [24] using $\tau^- \to \pi^-\pi^0\nu_\tau$ events. Here, the difference in efficiency for $M(\gamma\gamma)$ selection between data and MC samples is also added in quadrature to the systematic uncertainty.

The uncertainty due to the background model shown in Fig. 5 is estimated by changing it to a second-order polynomial and a fourth-order polynomial. We estimate the systematic uncertainty resulting from the signal functions by performing one thousand fits, in which we vary the lineshape parameters fixed from the signal MC samples, within their respective statistical uncertainties. The systematic uncertainty is the standard deviation of the fit results. The quadratic sum of the systematic uncertainties arising from the background model and the signal function is referred to as "fit function" in Table I.

TABLE I. Sources of systematic uncertainties for the relative branching fraction, $\mathcal{B}(\Lambda_c^+ \to pK_S^0\pi^0)/\mathcal{B}(\Lambda_c^+ \to pK^-\pi^+)$.

Sources	Value (%)
K_S^0 reconstruction	1.57
π^0 reconstruction	1.54
Fit function	0.60
MC statistics	0.58
Dalitz plot binning	0.68
PID of K^- and π^+	0.34
Tracking of K^- and π^+	0.70
Total	2.57

We include the statistical uncertainty of the signal MC samples used in the efficiency corrections across the Dalitz plots as a systematic uncertainty. We estimate the systematic uncertainties arising from the size of the Dalitz bins by modifying the Dalitz binning from the initial configuration of 5×10 to include the following configurations: 4×8, 4×10, 5×8, 5×12, 6×10, and 6×12. The largest difference obtained is attributed to a corresponding systematic uncertainty.

The systematic uncertainty from K^- and π^+ PIDs in $\Lambda_c^+ \to pK^-\pi^+$ decay is calculated based on the $D^{*+} \to D^0\pi^+(D^0 \to K^-\pi^+)$ control sample. Similar to the K_S^0 reconstruction, the PID efficiency as a function of momentum and polar angle in the laboratory frame is compared between data and MC samples. The systematic uncertainty attributed to tracking is 0.35% for each K^- and π^+ track in $\Lambda_c^+ \to pK^-\pi^+$ decay.

The uncertainties in the PDG values of $\mathcal{B}(\pi^0 \to \gamma\gamma)$ and $\mathcal{B}(K_S^0 \to \pi^+\pi^-)$ in Ref. [21] are negligible, so these contributions are not included in the systematic uncertainty. Other systematic uncertainties cancel out for the relative branching fraction measurements due to the similar kinematic distributions of the final state particles from $\Lambda_c^+ \to pK_S^0\pi^0$ and $\Lambda_c^+ \to pK^-\pi^+$ decays.

VII. SUMMARY

We study the $\Lambda_c^+ \to pK_S^0\pi^0$ decay using the full Belle dataset of 980 fb^{-1} at or near the $\Upsilon(nS)(n = 1, 2, 3, 4,$ and $5)$ resonances. The branching fraction of $\Lambda_c^+ \to pK_S^0\pi^0$ relative to $\Lambda_c^+ \to pK^-\pi^+$ is determined as

$$\frac{\mathcal{B}(\Lambda_c^+ \to pK_S^0\pi^0)}{\mathcal{B}(\Lambda_c^+ \to pK^-\pi^+)} = 0.339 \pm 0.002 \pm 0.009, \tag{6}$$

where the uncertainties are statistical and systematic, respectively. Using the PDG value of $\mathcal{B}(\Lambda_c^+ \to pK^-\pi^+) = (6.26 \pm 0.29)\%$ in Ref. [21], we obtain the following absolute branching fraction for $\Lambda_c^+ \to pK_S^0\pi^0$:

$$\mathcal{B}(\Lambda_c^+ \to pK_S^0\pi^0) = (2.13 \pm 0.01 \pm 0.05 \pm 0.11)\%, \tag{7}$$

where the uncertainties are statistical, systematic from this experiment and analysis, and due to the uncertainty in $\mathcal{B}(\Lambda_c^+ \to pK^-\pi^+)$, respectively. The measured branching fraction is consistent with the previous measurement by CLEO and has a fivefold improvement in precision [13].

Assuming isospin symmetry, we calculate that the ratio of the isospin amplitudes for $I = 1$ to $I = 0$ in the $N\bar{K}$ system is determined to be $1.23 \pm 0.03 \pm 0.06$, and the relative phase difference is obtained to be $1.842 \pm 0.001 \pm 0.069$, where the first uncertainty denotes the total uncertainty and the second uncertainty is from $\mathcal{B}(\Lambda_c^+ \to n\bar{K}^0\pi^+)/\mathcal{B}(\Lambda_c^+ \to pK^-\pi^+)$. These values are consistent with previous results [3]. However, we do not find a strong enhancement due to Σ^* resonances in the $M(pK_S^0)$ distribution of $\Lambda_c^+ \to pK_S^0\pi^0$ decay. These results indicate that factors beyond isospin symmetry, such as resonant contributions, cannot be neglected.

In addition, we observe a clear peaking structure in the $p\pi^0$ system near the $p\eta$ threshold, which may be attributed to a threshold cusp enhanced by $N(1535)^+$. Further amplitude analysis is required to understand the contributions of intermediate resonances such as K^*, Λ^*, Σ^*, Δ^*, and N^* resonances, as well as to estimate the non-resonant contribution. Such a comprehensive approach will lead to stringent tests of isospin symmetry by comparing the partial branching ratios between $\Lambda_c^+ \to pK^-\pi^+$ and $\Lambda_c^+ \to pK_S^0\pi^0$ decays. This approach could also contribute to a better understanding of non-factorizable processes in the non-leptonic decay of charmed baryons.

[1] Unless otherwise noted, charge-conjugate modes are always implied throughout this paper.

[2] C. D. Lü, W. Wang and F. S. Yu, Phys. Rev. D **93**, 056008 (2016).

[3] M. Ablikim *et al* (BESIII Collaboration), Phys. Rev. Lett. **118**, 112001 (2017).

[4] M. Gronau and J. L. Rosner, Phys. Rev. D **97**, 116015 (2018); M. Gronau, J. L. Rosner, and C. G. Wohl, Phys. Rev. D **98**, 073003 (2018).

[5] K. Miyahara, T. Hyodo and E. Oset, Phys. Rev. C **92**, 055204 (2015).

[6] J. K. Ahn *et al*, Phys. Rev. D **100**, 034027 (2019).

[7] Y. K. Hsiao, Q. Yi, S.-T. Cai, and H. J. Zhao, Eur. Phys. J. C **80**, 1067 (2020).

[8] R. Pavao, S. Sakai, and E. Oset, Phys. Rev. C **98**, 015201 (2018); E. J. Garzon and E. Oset, Phys. Rev. C **91**, 025201 (2015).

[9] S. B. Yang *et al.* (Belle Collaboration), Phys. Rev. Lett. **117**, 011801 (2016).

[10] S. B. Yang *et al.* (Belle Collaboration), Phys. Rev. D. **108**, L031104 (2023).

[11] X.-H. Liu, G. Li, J.-J. Xie, and Q. Zhao, Phys. Rev. D. **100**, 054006 (2019).

[12] M. J. Savage and R. P. Springer, Phys. Rev. D **42**, 1527 (1990).

[13] M. S. Alam *et al.* CLEO Collaboration, Phys. Rev. D **57**, 4467-4470 (1998).

[14] S. Kurokawa and E. Kikutani, Nucl. Instrum. Methods Phys. Res., Sect. A **499**, 1 (2003), and other papers included in this volume; T. Abe *et al.*, Prog. Theor. Exp. Phys. (**2013**), 03A001, and references therein.

[15] A. Abashian *et al.* (Belle Collaboration), Nucl. Instrum. Methods Phys. Res., Sect. A **479**, 117 (2002); also see detector section in J. Brodzicka *et al.*, Prog. Theor, Exp. Phys. (**2012**), 04D001.

[16] D. Lange, Nucl. Instrum. Methods Phys. Res., Sect. A **462**, 152 (2001).

[17] T. Sjöstrand, S. Mrenna, and P. Skands, J. High Energy Phys. 05 (2006) 026.

[18] R. Brun *et al.*, CERN Report No. DD/EE/84-1, 1984.

[19] E. Barberio and Z. Was, Comput. Phys. Commun. **79**, 291 (1994).

[20] H. Nakano *et al.* (Belle Collaboration), Phys. Rev. D **97**, 092003 (2018).

[21] R. L. Workman *et al.* (Particle Data Group), Prog. Theor. Exp. Phys. 2022, 083C01 (2022).

[22] L. K. Li *et al.* (Belle Collaboration), Phys. Rev. D **107**, 032004 (2023).

[23] J. Y. Lee *et al.* (Belle Collaboration), Phys. Rev. D **103**, 052005 (2021).

290 [24] S. Ryu *et al.* (Belle Collaboration), Phys. Rev. D **89**, 072009 (2014).